Article

In Situ Studies on Phase Transitions of Tris(acetylacetonato)-Aluminum(III) Al(acac)$_3$

Nicole Pienack, Laura Ruiz Arana, Wolfgang Bensch and Huayna Terraschke *

Institute of Inorganic Chemistry, University of Kiel, Max-Eyth-Str. 2, 24118 Kiel, Germany; pienack@ac.uni-kiel.de (N.P.); stu112651@mail.uni-kiel.de (L.R.A.); wbensch@ac.uni-kiel.de (W.B.)
* Correspondence: hterraschke@ac.uni-kiel.de; Tel.: +49-431-880-2402; Fax: +49-431-880-1520

Abstract: In situ investigations on the nucleation and crystallization processes are essential for understanding of the formation of solids. Hence, the results of such experiments are prerequisites for the rational synthesis of solid materials. The in situ approach allows the detection of precursors, intermediates, and/or polymorphs, which are mainly missed in applying ex situ experiments. With a newly developed crystallization cell, simultaneous in situ experiments with X-ray diffraction (XRD) and luminescence analysis are possible, also monitoring several other reaction parameters. Here, the crystallization of the model system tris(acetylacetonato)-aluminum(III) Al(acac)$_3$ was investigated. In the time-resolved in situ XRD patterns, two polymorphs of Al(acac)$_3$, the α- and the γ-phase, were detected at room temperature and the influence of the pH value onto the product formation was studied. Moreover, changes in the emission of Al(acac)$_3$ and the light transmission of the solution facilitated monitoring the reaction by in situ luminescence. The first results demonstrate the potential of the cell to be advantageous for controlling and monitoring several reaction parameters during the crystallization process.

Keywords: in situ studies; crystallization; in situ XRD; in situ luminescence; model system Al(acac)$_3$

1. Introduction

The objectives of chemical syntheses are the preparation and development of (novel) materials with special or even improved properties. Rational syntheses require a comprehensive understanding of the formation mechanisms of the compounds as well as of the synthetic procedures. For chemical reactions in fluid media, the prediction of synthesis products as well as reaction pathways are often challenging or, in most of the cases, impossible. Whereas the properties of crystalline solids are induced by the chemical composition and crystal structures (structure-properties-relationship), the processes like pre-organization, aggregation, nucleation, and crystal growth are often a mystery. If all steps occurring from the early stages of nucleation until the final product formation are known and well understood, a rational synthesis may be possible. To enhance the knowledge of chemical reaction processes, two approaches are applied: ex situ and in situ analyses of chemical reactions. In the ex situ approach, the reaction is quenched after distinct time intervals, followed by isolation and characterization of the products. Obviously, a huge number of experiments is needed, which is time consuming and costly. In addition, there is no guarantee that the quenched products reflect the real stage of the reaction, because the quenching and/or working-up procedures might influence the results yielded in different products and therefore lead to wrong conclusions. In situ experiments have the advantage that processes can be studied without disturbing the reaction system, but while continuously monitoring and detecting as much reaction data as possible. Therefore, in situ investigations of the formation of (crystalline) solids are necessary for a better understanding of the different processes

occurring during the reaction. In situ investigations allow the detection of crystalline precursors, intermediates, and/or polymorphs which may be overlooked using the ex situ approach [1].

With our crystallization cell, monitoring and controlling of the synthesis conditions and reaction parameters during chemical reactions in fluid media can be realized. The knowledge of parameters—like temperature, pressure, pH value, redox potential, and conductivity—is crucial for controlling the formation and growth of (crystalline) materials. Combined with Attenuated Total Reflectance Fourier Transform Infrared (ATR-FT-IR) spectroscopy, the species present in solution can be identified. Further modifications of the cell setup offer the possibilities of simultaneous in situ experiments with X-ray diffraction (XRD) and in situ luminescence analysis [2–5].

Results of in situ XRD investigations permit formulation of kinetic models of the crystal growth. In recent years/decades, several publications highlighted the results of various in situ studies, especially with in situ X-ray scattering experiments [1,6–31]. Observations of the formation of intermediate phases or polymorphs and the transformation into the final products are possible with in situ XRD. With synchrotron radiation, XRD patterns can be collected in short time scales (up to a few seconds) and due to the high energy, intensity, and brilliance of the radiation also special conditions and sample environments can be used. For such in situ experiments, our cell was modified (details in Materials and Methods), the setup was tested and successfully applied at synchrotron radiation facilities [32].

The crystallization of tris(acetylacetonato)-aluminum(III) $Al(acac)_3$ was chosen as the model system for in situ XRD and simultaneous luminescence analysis. $Al(acac)_3$, also known as aluminum acetylacetonate, occurs as various polymorphs: the thermodynamically stable α-phase [33], the γ-polymorph [34] or the δ-phase (observed at 110 K, superstructure of the α-polymorph) [35]. In several publications, the structures of the polymorphs and their properties were reported, e.g., the synthesis and crystal structure [36], Density Functional Theory (DFT) calculations to probe the crystal structure of the polymorphs [37], crystal structure and luminescence [38], thermal cell-expansion (under light irradiation) [39], luminescence of $Al(acac)_3:Cr^{3+}$ [40], thermodynamics of sublimation of $Al(acac)_3$ [41], just to name a few. The huge number of papers is due to possible applications, i.e., $Al(acac)_3$ is a common precursor for the preparation of alumina Al_2O_3, [36,42–44] for thin films via CVD [45,46] or nanoparticles [42] and several polymers, e.g., polycarbosilanes (PACS) [47,48]. It is also used as charging additive for liquid electrostatic toners [49] and as additive for perowskite precursor solutions improving crystal quality and reducing strain in the films for perowskite solar cells [50].

As mentioned above, $Al(acac)_3$ is chosen as model system to demonstrate the performance of the in situ cell, especially the modified reactor system (details in Materials and Methods). Herein, we present the results of the in situ XRD studies and in situ luminescence analysis obtained during the crystallization of $Al(acac)_3$.

2. Results and Discussion

For studying the crystallization of $Al(acac)_3$, the syntheses were performed in adapted glass vessels under stirring, while several reaction parameters were monitored simultaneously. In subsequent in situ XRD studies with combined in situ luminescence analysis, the crystallization of $Al(acac)_3$ was studied at beamlines P07B and P09 at PETRA III (Positron-Elektron-Tandem-Ring-Anlage III), German Electron Synchrotron (Deutsches Elektronen Synchrotron (DESY)) in Hamburg (details in Section 3). During the formation of the product, the changes of different parameters, e.g., pH value and redox potential were monitored and the species in solution identified with ATR-FT-IR spectroscopy.

2.1. Phase Transitions of Al(acac)₃

The growth of the Bragg reflections during the crystallization of $Al(acac)_3$ is shown in the time-resolved in situ XRD patterns (Figure 1a). After a short induction time (the time until the first reflections are observable), the intensity of the reflections start to grow during the addition of NH_3

solution. Selected powder patterns after certain reaction times (10, 20, 30, and 75 min) are presented in Figure 1b.
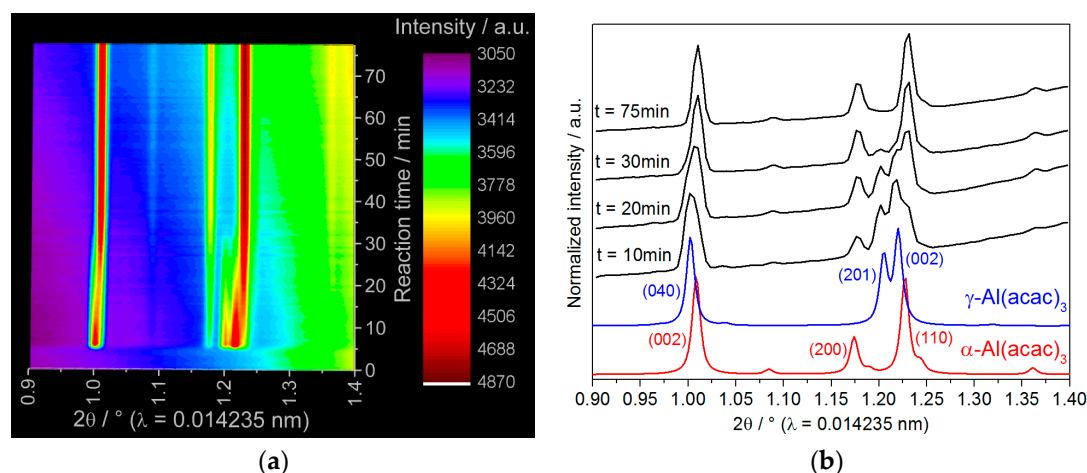
Figure 1. (**a**) Time-resolved XRD patterns during the formation of Al(acac)$_3$, recorded at the PETRA III beamline P07B (room temperature, concentration of NH$_3$ 25%); (**b**) XRD pattern after 10, 20, 30, and 75 min of reaction time and the calculated patterns of the polymorphs [33–35].

Interestingly, two phases are detected in the beginning of the reaction and the stable α-phase is observed at the end of the experiments (Figure 1b). Starting the reaction, reflections of the γ-phase of Al(acac)$_3$ as well as weak reflections caused by the α-phase are visible after the induction time of five minutes. During the reaction progress, the intensity of the reflections of the α-phase grows and the intensity of these reflections increases on cost of the γ-polymorph (see Figure 1a). Comparing the normalized intensities of the reflections at 1.176 2θ, assigned to the (200) reflection of α-Al(acac)$_3$, and at 1.202 2θ, assigned to the (201) Bragg reflection of γ-Al(acac)$_3$, an intersection at an extent of reaction α ≈ 0.5 (Figure S1) is observed, suggesting that the crystallization mechanism for the formation of the final product is rather determined by a solid-solid phase transition than an amorphization or partial dissolution of the γ-polymorph [17].

Al(acac)$_3$ is colorless under irradiation with day light, but emits blue light under UV irradiation (320 nm, Figure 2). This behavior is in agreement with the recorded luminescence spectra, in which the emission spectrum of Al(acac)$_3$ (λ$_{ex}$ = 320 nm, Figure S2) is extended between 400 nm and 700 nm, consisting of a combination of multiple bands, with maxima at 440 nm, 460 nm, and 509 nm, discussed very briefly in the work of Yu et al. [38]. Similarly, the excitation spectrum (λ$_{em}$ = 450 nm, Figure S2) consists of a broad band with the maximum at 328 nm. Applying the emission spectrum of Al(acac)$_3$ for calculating the coordinates for the Commission Internationale de L'éclairage chromaticity diagram CIE 1931 resulted in the values of x = 0.2017 and y = 0.3313 (Figure S3, [51]). Pure acetylacetone, on the other hand, presents a very weak luminescence, where the emission spectrum (λ$_{ex}$ = 380 nm, Figure S4) is composed by a broad band between approximately 417 nm and 833 nm, with the maximum at 550 nm, while the maximum of the respective excitation spectrum is located at 465 nm. These large differences between the optical properties of uncoordinated acetylacetone and as ligands bonded to Al^{3+} in Al(acac)$_3$ allows monitoring the crystallization process by means of in situ luminescence measurements.

As shown in Figure 3a, the in situ luminescence spectra recorded during crystallization of Al(acac)$_3$ adding conc. NH$_3$ (25%) to the aqueous solution of Al(NO$_3$)$_3$·9H$_2$O and acac results in a drastic increase of the emission intensity after approximately 2.1 min, corresponding to the addition of 1.06 mL resp. ca. 14 mmol of NH$_3$. At t = 3.2 min, the emission intensity starts to decrease, continuously decreasing nearly constantly until the end of the reaction, with exception of the oscillation at approximately t = 20–30 min, coinciding with the reaction time at which the transition between the α- and γ-phases was detected by the in situ XRD experiments (Figure 1). No shift of the emission band has been

detected during the phase transition of Al(acac)$_3$, probably due to the similarity of the structures of the polymorphs. Since only the intensity of the emission varies during the phase transformation, additional experiments recording in situ excitation spectra must be carried out in order to explain this phenomenon.
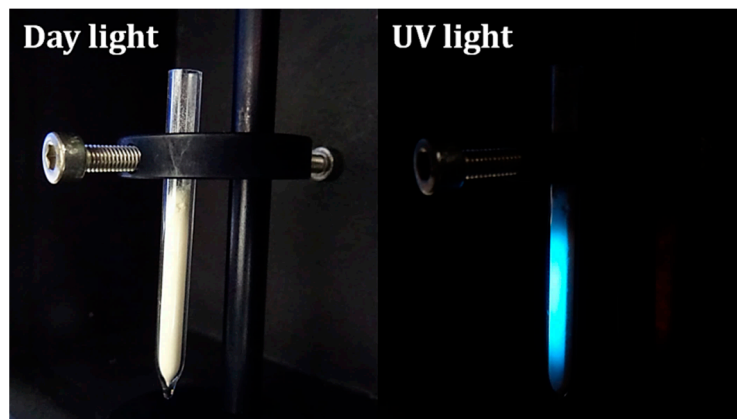
Figure 2. Suprasil quartz ampoule containing Al(acac)$_3$ crystallized with 25% NH$_3$ under irradiation of day (left-hand side) and UV (320 nm, right-hand side) light.

| (**a**) | (**b**) |
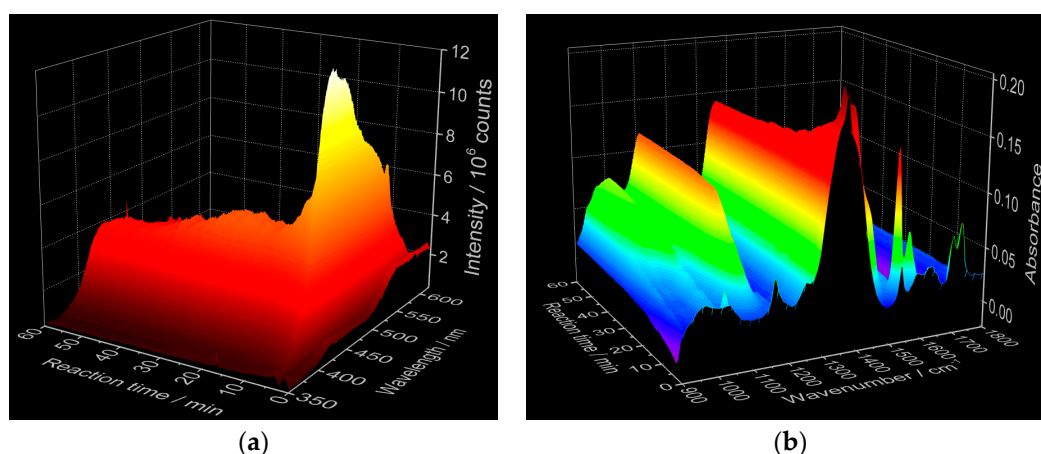
Figure 3. (**a**) In situ luminescence and (**b**) infrared spectroscopic analysis during the crystallization of Al(acac)$_3$ (35 °C, concentration of NH$_3$ 25%).

The in situ IR spectra (Figure 3b) of the initial solution before the addition of NH$_3$ contain the NO$_3^-$ vibrations at 1349 cm^{-1} and 1536 cm^{-1}, besides the acetylacetone-related absorptions at 1700 cm^{-1} and 1722 cm^{-1} (Figure S5) [52,53]. During the addition of NH$_3$, an increase of the NO$_3^-$ and a decrease of the acac-related vibrations are observed. The complex reaction processes occurring during the addition of 25% NH$_3$ to the Al(NO$_3$)$_3$ and acac solutions at t < 20 min are divided into three different periods, namely, A (t = 0–2.1 min), B (t = 2.1–3.2 min), and C (t = 3.2–20 min). In order to illustrate the changes in the reaction system, the evolutions of key parameters during these periods have been selected and are shown in Figure 4. These key parameters are: the intensity of the Al(acac)$_3$ emission band at 450 nm, the pH value, redox potential and the absorbance of the acac, NO$_3^-$ and NH$_3$ [54] vibrations at 1722 cm^{-1}, 1536 cm^{-1}, and 1115 cm^{-1}, respectively. Period A occurs between the reaction time t = 0 and t ≈ 2.1 min, where ca. 14 mmol NH$_3$ was added, causing the increase of the pH value up to 2.4. The acac IR mode starts to decrease, indicating the uptake of acac molecules from the solution for the formation of the Al(acac)$_3$ complex. The release of the NO$_3^-$ anions during the reaction

is evidenced by the increase of the IR signal and the decrease of the redox potential. The NH_3 related IR signal slightly decreases, probably due to its consumption during the reaction. The enhancement of the NO_3^- IR absorption may be explained by the release of this ion from the solvation sphere around Al^{3+} into the solution for the formation of the $Al(acac)_3$ complex. The simultaneous change of nearly all parameters at t = 1.1 min might indicate the moment where the $Al(acac)_3$ complex is formed but still remains dissolved in the solvent. Up to the end of reaction period A, the emission band at 450 nm is not observed yet, strongly growing afterwards until the end of the reaction period B at t = 3.2 min, indicating the beginning of crystallization of $Al(acac)_3$. Due to the formation of the solid material, the luminescent complex is less subjected to solvent quenching effects [55], resulting in the enhancement of the emission intensity. Therefore, this experiment suggests that the addition of approximately 14 mmol NH_3 and the simultaneous increase of the pH value to 2.4 are the critical conditions leading to the precipitation of the solid $Al(acac)_3$ material. The formation of solid $Al(acac)_3$ apparently lasts until the beginning of reaction period C at 3.2 min, where the acac related IR signal is stabilized, implying that the acac molecules are no longer removed from the solution, and the redox potential stops decreasing while the pH value now remains mainly constant. After the solid material is nearly completely formed at the beginning of the reaction period C, NH_3 is no longer consumed by the chemical reaction, and the respective IR signal increases with further addition of NH_3 solution.
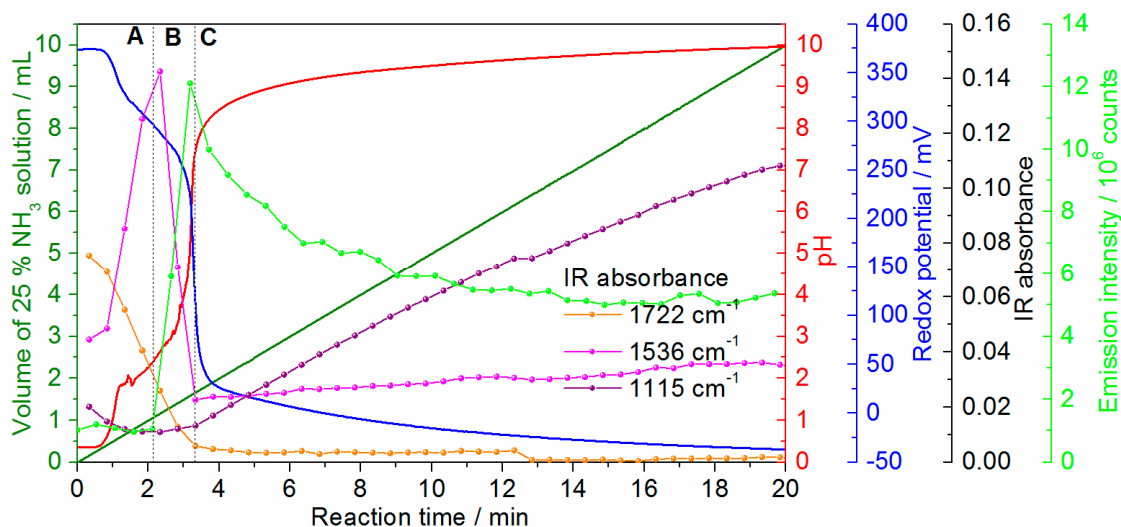
Figure 4. Dependence of the redox potential (blue curve), pH (red curve) emission intensity at 450 nm (light green curve, λ_{ex} = 320 nm) as well as IR absorbance at 1722 cm^{-1} (orange dots), 1536 cm^{-1} (pink dots), and 1115 cm^{-1} (purple dots) on the addition of the 25% NH_3 solution.

2.2. Influence of the NH_3 Concentration

The knowledge of the critical synthesis conditions leading to the precipitation of $Al(acac)_3$ allows altering the reaction parameters in order to manipulate the crystallization time according to the concentration of the added NH_3 solution. Here, the beginning of the crystallization has been determined by means of in situ luminescence analysis, monitoring the intensity of the blue emission band at 450 nm when excited at 320 nm (Figure 5a), confirming the results by comparison with in situ IR analysis (Figure 5b). As discussed above, the induction time at t = 2.1 min during the addition of 25% NH_3 solution is detected by a rapid increase of the emission intensity. Decreasing the NH_3 concentration to 12.5%, the emission intensity starts to increase only after 3.7 min (Figure S6), suggesting a delay of the crystallization as well as the induction time to the moment when the amount of NH_3 approaches the critical concentration and a pH value of 2.5 (Figure S7), as discussed above. The slight difference between the pH values at the induction times can be explained with experimental variations comparing results of different experiments. Decreasing the NH_3 concentration

to approximately 3.5%, the emission intensity starts to increase only after 11.2 min. at pH = 2.5 (Figure S8), confirming the successful control of the crystallization/induction time by means of the NH_3 concentration and, consequently, the pH value. Similarly, as explained above (see Figure 3), the stabilization of the absorbance of the IR mode of the acac molecule at 1722 cm^{-1} (Figure 5b) after approximately 3.3, 5.9, and 17.3 min suggests the end of the crystallization processes for the reactions applying respectively 25%, 12.5%, and 3.5% NH_3, when the acetylacetone ligands are no longer removed from the solution for the formation of the solid material (Figure S9). The end of the crystallization process is also noticed in the in situ luminescence measurements, when the emission intensity at 450 nm stops to grow. Comparable to the reaction carried out with 25% NH_3 solution, the oscillation of the emission intensity for 12.5% and 3.5% NH_3 in the range of t ≈ 20–40 min could be related to the transformation between the γ- and α-polymorphs, but was not investigated in detail yet as well as the decrease of emission intensity for 25% NH_3 after t = 44 min.

The instability of the γ-Al(acac)$_3$ and its conversion to the most stable α-phase is shown in addition by the attempt to carry out ex situ X-ray diffraction analysis for reactions performed with 12.5% and 25% NH_3 (Figure S10). Even though samples removed from the reactor for t < 20 min were expected to contain γ-Al(acac)$_3$ according to the in situ XRD measurements, this phase was most probably converted during the removal from the reaction and/or quenching and/or the drying process. Consequently, only the α-phase could be detected by ex situ XRD, reinforcing the importance of in situ experiments for efficiently characterizing this system and proving the assertion mentioned in the introduction that quenched products not always reflect the real reaction state. The working up process yields in the thermodynamically stable α-phase, and without the means of in situ XRD the phase transition would not be monitored.
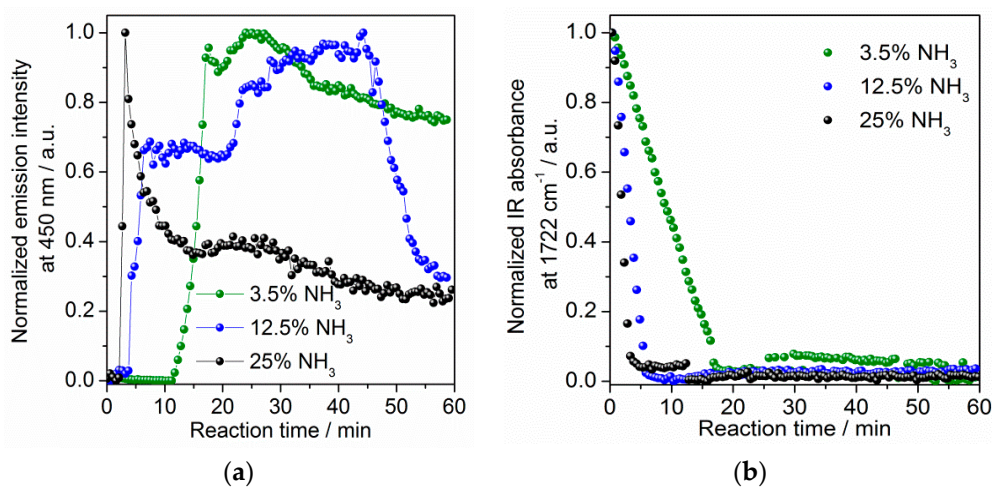
Figure 5. (**a**) Emission intensity at 450 nm and (**b**) infrared absorbance at 1722 cm^{-1} for NH_3 concentrations of 25% (black dots), 12.5% (blue dots), and 3.5% (green dots).

2.3. Detection of Crystallization by Light Transmission

Besides in situ fluorescence measurements, other optical properties can also be used for detecting the crystallization of solid materials. It is demonstrated that monitoring the changes in the transmission of light through the reaction solution offers the possibility for sensing the increase of the turbidity caused by the formation of solid materials. The advantage of this approach is that the induction time can be estimated, independent of the luminescence ability and also nearly independent of the energy of the light source, increasing the flexibility of its application. For these experiments, a 395 nm LED was applied as light source, irradiating the reactor from outside, while its intensity through the reaction medium was continuously measured by means of an optical fiber connected to a Charge-Coupled Device (CCD) detector (StellarNet Inc., Tampa, FL, USA) and submersed in the reactor. Figure 6a

displays the dependence of the intensity of the light on the reaction time. Starting the addition of 25% NH_3, the intensity of the light source strongly decreases after 3 min (Figure S11a), indicating the beginning of crystallization at this time, comparable to the results shown in Figures 4 and 5 for in situ luminescence, pH value, redox potential and IR spectroscopy measurements. The early stages of crystallization detected by the transmission of the light were also confirmed by the simultaneous in situ X-ray diffraction analysis performed at the beamline P09 at DESY, where the induction time coincides with the increase of the intensity of the reflections of $Al(acac)_3$ (Figure S11b). The posterior decrease of the solution turbidity implied by the enhancement of the intensity of the light transmitted through the solution coincides with the decrease of the intensity of the $Al(acac)_3$ reflections. However, the reflections measured at P09 were very broad, causing a strong overlap between the reflections assigned to the α- and γ-phases. Therefore, it was not possible to assign the reflections related to the individual phases for comparing their intensities quantitatively. The decrease in the turbidity of the reaction medium suggests a partial dissolution of the product, indicating the solid-solid phase transformation between the $Al(acac)_3$ polymorphs discussed above might not be the only mechanism ruling this reaction, since additionally the most stable α-phase is also formed in parallel to γ-$Al(acac)_3$ in the beginning of the reaction. The partial dissolution of the solid material suggested here would explain the decay of the emission intensity at 450 nm (Figure 5a) after the crystallization process.
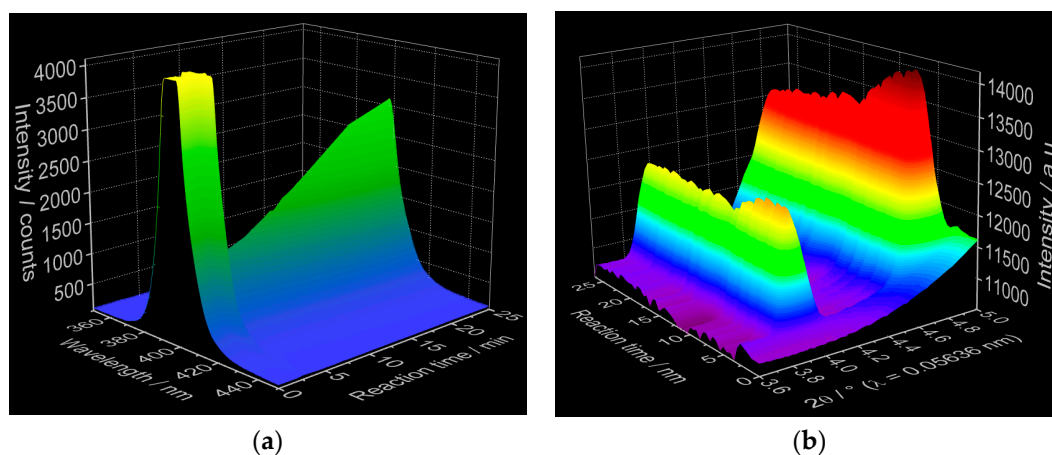
Figure 6. (**a**) Light transmission detected by the intensity at 395 nm through the reaction medium and (**b**) in situ XRD of $Al(acac)_3$ crystallized with NH_3 solution (35 °C, concentration of NH_3 25%).

Decreasing the concentration of the ammonia solution to 12.5%, the offset of the decay of the light transmission is delayed to t ≈ 4 min (Figure S12), indicating also a shift in the induction time, similarly to the previous experiments measuring in situ pH value, redox potential, IR and fluorescence spectra. As expected, the results of these experiments are supplementary confirmed by the simultaneous increase of the intensity of Bragg reflections of $Al(acac)_3$ (Figure S13). In contrast to the reaction carried out applying 25% NH_3, the turbidity of the solution with 12.5% NH_3 does not decrease after crystallization (Figure S14). This observation suggests that the product is not partially dissolved under these reaction conditions, in agreement with the stabilization of the emission intensity after crystallization shown in the Figure 5a (blue curve, t ≈ 6 min). Interestingly, for the reaction carried out by the addition of 2.5% NH_3, no reflection could be detected in the in situ XRD patterns during the reaction time of 25 min. However, a decrease of the light transmission and therefore an increase of the turbidity of the reaction medium are observed (Figures S12 and S14). This phenomenon suggests that additional processes occur in the reaction suspension, which cannot be detected by XRD.

In this context, three possible hypotheses may explain this phenomenon: (i) the formation of $Al(acac)_3$ which remains in solution and does not reach the critical concentration in order to precipitate; (ii) the formed crystals are too small or their concentration is too low; or (iii) the formation

of an amorphous phase which lacks long-range order prevents the characterization by means of XRD analysis. Additional investigations are necessary for verifying which of these assumptions explains such experimental results. Contrary to the beginning of the induction process, the conversion between γ- and α-phases apparently does not depend strongly on the NH_3 concentration but more on the reaction time. Here, for 12.5% or 25% NH_3, the growth of the α-phase is preferred for reaction time t > 20 min (Figures S11 and S13).

3. Materials and Methods

The experiments presented here were performed with our newly designed crystallization cell (Figures S15 and S16). This set-up allows the detection and the control of different reaction parameters during chemical reactions in fluid media. The knowledge of reaction parameters, such as temperature, pressure, pH value, redox potential, and/or conductivity, is critical for the formation of crystalline solids. Combining the data of different sources with ATR-FT-IR spectroscopy, the species present in the reaction solutions and their concentrations can be identified and determined, respectively.

The synthesis workstation EasyMax® 102 (Mettler Toledo, Gießen, Germany) is an automated reactor system for performing synthesis in parallel in different glass vessels or pressure reactors. The temperature range from $-25\,^{\circ}C$ up to $180\,^{\circ}C$ is realized by the solid-state thermostat, the control is reached with Pt100 sensors and several sensors/electrodes can be adapted by using a universal control box (UCB). The operation can be done by a touchpad as well as by the iControl EasyMax® software (Mettler Toledo, Gießen, Germany).

ATR-FT-IR spectra are collected with the ReactIR™ 45 m spectrometer (Mettler Toledo, Gießen, Germany) with a 6.3 mm AgX fiber (1.5 m length) as probe module, a diamond probe sensor, and a measurement range of 1950–650 cm^{-1}. The iC IR™ (Mettler Toledo, Gießen, Germany) software allows the evaluation of the data.

Details and performance characteristics of the in situ cell and the equipment are presented in Table 1. Additional figures can be obtained from supporting materials.

Table 1. Selected data of the in situ crystallization cell.

Features/Facilities	Options
Synthesis workstation EasyMax® (Mettler Toledo)	Automated lab system with two reactor positions for different reaction vessels with integrated heating and cooling
Temperature range	-25 up to $180\,^{\circ}C$, jacket temperature (solid state thermostat)
Temperature control	External and/or internal; constant rates or ramps
Reaction vessels	Glass vessels (V_{max} = 50/100 mL), stainless steel pressure vessels (V_{max} = 80 mL; Parr Instruments)
Dosing	Dosing unit and dosing pumps for both positions
Stirring	Magnetic and/or mechanical stirrers (steel, glass); up to 1000 rpm
Probes/sensors	pH value, redox potential, conductivity, ATR-FT-IR spectroscopy (ReactIR™ 45 m (Mettler Toledo))
Modifications	In situ (energy-dispersive) X-ray diffraction ((ED)XRD), in situ luminescence analysis of coordination sensors (ILACS)

3.1. Modifications

For in situ XRD experiments, the assembly needed to be varied, e.g., the volumes of the glass reactors were too big, and so the scattering volumes should be decreased for sufficient signal-to-noise ratios. Pre-examinations proved glass tubes or flow cells with approx. 1 cm in diameter as suitable scattering ranges/volumes, but external circuits were not convenient. Our modified reaction vessel features a small glass tube fixed inside, so that the scattering volume is in an acceptable range (Figure S17a). A special sample holder (Figure S17b) [56] for temperature control (via heating wires) completes this setup and it was successfully adapted at several beamlines at synchrotron

radiation facilities (Figure S18 and Figure S19). Selected pictures of the setup are presented as supporting materials.

3.2. Synthesis

All chemicals were used as purchased without further purification. $Al(NO_3)_3 \cdot 9H_2O$ ($\geq$98.5%, CAS 7784-27-2, Merck, Darmstadt, Germany), acetylacetone ($C_5H_8O_2$, $\geq$99%, CAS 123-54-6, Merck, Darmstadt, Germany), and NH_3 (25%, CAS 7664-41-7, Walter CMP, Kiel, Germany) were dissolved in water. A typical reaction starts with 1.875 g (0.50 mmol) $Al(NO_3)_3 \cdot 9H_2O$ in 25 mL water (50 mL glass reactor, T = 35 °C, r = 300–500 rpm, sensors for pH value and redox potential), adding 1.625 mL (0.016 mmol) acetylacetone and waiting five minutes until the signal of the sensors are constant. Then, 10 mL diluted ammonia (3.5%–25%) were added with a rate of 0.5 mL/min. The reaction products were centrifuged, dried at 80 °C for few hours and the crystalline powders are characterized via ex situ X-ray diffraction.

3.3. X-ray Diffraction Experiments

Ex situ XRD data were collected on a STOE Stadi-p X-ray powder diffractometer (STOE & Cie GmbH, Darmstadt, Germany) with Cu $K_{\alpha 1}$ radiation (λ = 1.54056 Å; Ge monochromator; flat samples) in transmission geometry with an IP-PSD (STOE & Cie GmbH, Darmstadt, Germany) and/or a DECTRIS® MYTHEN 1K detector (DECTRIS, Baden-Daettwil, Switzerland).

The in situ XRD experiments were done at the PETRA III beamlines P07B [57] and P09 [58] at German Electron Synchrotron DESY in Hamburg. Similarly, as for the experiments carried out in the in situ crystallization cell in Kiel, in typical experiments, the solution of 1.875 g (0.50 mmol) $Al(NO_3)_3 \cdot 9H_2O$ and 1.625 mL (0.016 mmol) acetylacetone in 25 mL water was placed inside the modified glass reactor (V_{max} = 50 mL) and 10 mL of 2.5%–25% NH_3 solution was added with a pump system (two 5 mL syringes in parallel addition with 0.25 mL/min). For the experiments at the DESY beamline P09, the total volume of added ammonia solution was decreased to 9 mL. The reactions were carried out at the local room temperature, resulting in a temperature inside the reactor of approximately 35 °C. The scattered signals were collected at DESY with a Perkin Elmer XRD1621 detector (PerkinElmer Technologies, Walluf, Germany) (2048 × 2048 pixels, X pixel size 200.00 mm, Y pixel size 200.00 mm) with a measurement time of 30 s per diffractogram. At beamline P07B, the energy was 87.1 keV, with the respective wavelength of 0.14235 Å, and the detector distance was about 2683 mm. Experiments carried out at the beamline P09 applied the energy of 22 keV (0.5636 Å) and a detector distance of 555 mm.

3.4. In Situ Luminescence Analysis

In situ luminescence experiments at the University of Kiel were performed with a FL322 Fluorolog-3 fluorescence spectrometer (HORIBA Jobin Yvon GmbH, Unterhaching, Germany), equipped with a R928P Photomultiplier, iHR-320-FA triple grating imaging spectrograph, a Syncerity charge-coupled device (CCD) detector and a 450 W xenon lamp. A Y-shaped optical fiber was used for transmitting the excitation light from the spectrometer to the reactor content as well as the emitted light from the reactor to the CCD detector, recording one luminescence spectrum every 30 s.

The dependence of the light transmission and turbidity of the mother solution during crystallization of $Al(acac)_3$ in parallel to in situ XRD at the DESY facilities was studied combining a 395 nm LED (Wha Fat Technological Co. Ltd, Shenzhen, China) with a portable EPP2000 (StellarNet Inc., Tampa, FL, USA) spectrometer, equipped with a CCD-based detector. The UV LED was used for irradiating the solution through an observation window outside the reactor, while the intensity of the transmitted light was detected by an optical fiber attached to the EPP2000 spectrometer.

4. Conclusions

The results of the experiments demonstrate the large potential of the in situ crystallization cell of the University of Kiel and the successful modifications for characterizing the crystallization process and phase transitions of the model system Al(acac)$_3$. For reaching this goal, different characterization methods have been combined and reaction parameters were monitored in situ like the pH value and redox potential. Most importantly, a new technique for investigating crystallization processes applying in situ luminescence measurements has been used, comparing the results with in situ X-ray diffraction experiments carried out at different beamlines at DESY (Hamburg). Preliminary in situ XRD investigations at the beamline P07B showed the simultaneous crystallization of the α- and γ-Al(acac)$_3$ polymorphs, followed by the subsequent conversion of the γ- to the most stable α-phase. Al(acac)$_3$ emits blue light under irradiation with UV light, resulting from an emission band with the maximum at 460 nm (λ_{ex} = 320 nm) and CIE 1931 color coordinates of x = 0.2017 and y = 0.3313. The difference of the optical properties between the Al(acac)$_3$ product and the starting material acetylacetone with a weak emission signal at 550 nm (λ_{ex} = 380 nm), allows the characterization of the synthesis monitoring the enhancement of the Al(acac)$_3$ emission at e.g., 450 nm. In situ emission spectra showed an induction time of 2.1 min adding 25% NH$_3$ to the aluminum nitrate and acetylacetone solution. The critical condition for initiation of the crystallization process was identified as pH $\approx$ 2.4 (14 mmol NH$_3$ solution (25%)). The knowledge of the critical parameter allowed the controlled delay of the induction time to t = 3.7 min and t = 11.2 min, decreasing the NH$_3$ concentration to 12.5% and 3.5%, respectively. Now, reaching the crystallization of Al(acac)$_3$ after the addition of only 14 mmol NH$_3$ represents a significant improvement of the conditions of the original experiments, which were performed adding 10 mL of 25% NH$_3$ solution (ca. 134 mmol). Finally, an alternative approach was demonstrated here, determining the induction time of Al(acac)$_3$ by analyzing the turbidity of the aqueous solution and comparing the results with in situ XRD data. The time-dependent turbidity analysis is advantageous compared to in situ luminescence because it is not limited to light emitting compounds and does not depend on the light excitation source, but is less sensitive. Additional information about the transition between the α- and γ-polymorphs can be acquired in the future applying the in situ luminescence analysis of coordination sensors (ILACS) approach [2], doping Cr^{3+} on the Al^{3+} sites, as already demonstrated ex situ in the literature [40], and monitoring the influence of the phase transformation on the intensity and also in the position of the Cr^{3+} emission spectra.

Supplementary Materials: The following are available online at www.mdpi.com/2073-4352/6/12/157/s1. Figure S1: Dependence of the addition of 25% NH$_3$ solution as well as normalized intensity of the reflections (λ = 0.14235 Å) of α-Al(acac)$_3$ (1.176 ° 2θ) and γ-Al(acac)$_3$ (1.202 ° 2θ) on the reaction time, measured at the Beamline P07B at DESY. Figure S2: Emission (blue curve, λ_{ex} = 310 nm) and excitation (black curve, λ_{em} = 450 nm) spectra of Al(acac)$_3$, crystallized by the addition of 25% NH$_3$ solution. Figure S3: CIE (Commission internationale de l'éclairage) 1931 chromaticity diagram, displaying the color coordinated of Al(acac)$_3$ (x = 0.2017, y = 0.3313), calculated from the emission spectrum of Figure S2, applying the Spectra Lux Software v.2.0 [51]. Figure S4: Emission (red curve, λ_{ex} = 380 nm) and excitation (black curve, λ_{ex} = 550 nm) spectra of pure acetylacetone. Figure S5: In situ IR spectra measured during crystallization with 25% NH$_3$ for reaction time t = 5–60 min, in comparison to starting solutions of NH$_3$ and aluminum nitrate with acetylacetone as well as pure acetylacetone. Figure S6: In situ luminescence spectra recorded during crystallization of Al(acac)$_3$ with (**a**) 12.5% and (**b**) 3.5% NH$_3$ solution (λ_{ex} = 320 nm). Figure S7: Dependence of the volume of 12.5% NH$_3$ solution (black curve), pH (red curve) and redox potential (blue curve) on the reaction time. Figure S8: Dependence of the volume of 3.5% NH$_3$ solution (black curve), pH (red curve) and redox potential (blue curve) on the reaction time. Figure S9: In situ IR spectra recorded during crystallization of Al(acac)$_3$ with (**a**) 12.5% and (**b**) 3.5% NH$_3$ solution. Figure S10: Ex situ XRD patterns of Al(acac)$_3$ measured after the removal of the sample by reaction time t = 5–60 min, centrifuging and drying for reactions with (**a**) 25% NH$_3$ and (**b**) 12.5% NH$_3$. Ex situ treatment causes complete conversion of the product to most stable α-phases, showing the importance of in situ XRD measured with synchrotron radiation. Figure S11: Comparison of (**a**) light (blue curve) and XRD (red curve) intensity in dependence of the addition of NH$_3$ during crystallization of Al(acac)$_3$ and (**b**) comparison of measured in situ XRD patterns with calculated patterns for the respective α- and γ-phases. Figure S12: (**a**) Light intensity of 395 nm LED transmitted through the reaction medium for the addition of (**a**) 12.5% NH$_3$ and (**b**) 2.5% NH$_3$ measured simultaneously to in situ XRD at the Beamline P09 at DESY. Oscillation of the light intensity is probably caused by mixing problems. Figure S13: (**a**) In situ XRD of Al(acac)$_3$ crystallized with a 12.5% NH$_3$ solution, measured at the beamline P09 at DESY, and (**b**) comparison of measured in situ XRD patterns with calculated patterns for the

respective α- and γ-phases. The asterisk (*) sign shows an artefact caused by the oscillation at the beam intensity. Figure S14: Comparison of light transmission intensity through the reaction solution for the crystallization of Al(acac)$_3$ by the addition of 2.5%, 12.5%, and 25% NH$_3$ solution. Figure S15: Setup of the crystallization cell in Kiel. The main parts of the equipment are marked. Figure S16: Adaptation of the crystallization cell in Kiel for in situ luminescence measurements. Figure S17: (**a**) Modified reaction vessel with a glass tube fixed inside; (**b**) Scheme of the special constructed sample holder (for the glass vessel (a)) for temperature control, stirring, additional sensors, XRD and luminescence measurements [56]; Figure S18: Experimental setup of the crystallization cell at the PETRA III beamline P07B, DESY, Germany. Here, the system is equipped with modified glass vessel for the scattering experiments (see figures below). Figure S19: Experimental setup of the crystallization cell at the DORIS beamline F3, HASYLAB, DESY, Germany. Here, the system is equipped with an external flow cell for the scattering experiments and a piston pump allowing the circulation of the reaction mixtures.

Author Contributions: Nicole Pienack and Huayna Terraschke wrote the article, designed the experiments and performed them at the synchrotron facilities. Laura Ruiz Arana performed the experiments at the in situ crystallization cell in Kiel and helped with the data analysis. Wolfgang Bensch provided the necessary material and equipment, and also supervised the experiments.

Conflicts of Interest: The authors declare no conflict of interest.

References and Notes

1. Pienack, N.; Bensch, W. In situ Monitoring of the Formation of Crystalline Solids. *Angew. Chem. Int. Ed.* **2011**, *50*, 2014–2034. [CrossRef] [PubMed]

2. Terraschke, H.; Ruiz Arana, L.; Lindenberg, P.; Bensch, W. Development of a new in situ analysis technique applying luminescence of local coordination sensors: Principle and application for monitoring metal-ligand exchange processes. *Analyst* **2016**, *141*, 2588–2594. [CrossRef] [PubMed]

3. Tsirigoni, A.-M.; Ruiz Arana, L.; Lindenberg, P.; Terraschke, H. In situ Monitoring of Calcium Phosphate Phase Transitions: A Spectroscopic Approach. *Z. Anorg. Allg. Chem.* **2016**, *1073*. [CrossRef]

4. Polzin, P.; Eliani, I.V.; Terraschke, H. Characterizing the Crystallization Kinetics of Ln(2,2-Bipyridine)$_2$(NO$_3$)$_3$ (Ln = Eu, Tb) by New in situ Luminescence Analysis Technique. *Z. Anorg. Allg. Chem.* **2016**, *1073*. [CrossRef]

5. Lindenberg, P.; Ruiz Arana, L.; Heidenreich, N.; Terraschke, H. Polymorphism and in situ Detection of Reaction Intermediates on Eu(1,10-Phenanthroline)$_2$(NO$_3$)$_3$. *Z. Anorg. Allg. Chem.* **2016**, *1074*. [CrossRef]

6. Seidlhofer, B.; Pienack, N.; Bensch, W. Synthesis of Inorganic-Organic Hybrid Thiometallate Materials with a Special Focus on Thioantimonates and Thiostannates and in situ X-ray Scattering Studies of Their Formation. *Z. Naturforsch.* **2010**, *65*, 937–975. [CrossRef]

7. Clark, S.M.; Evans, J.S.O.; O'Hare, D.; Nuttall, C.J.; Wong, H.-V. Real-time in situ X-ray diffraction of intercalation reactions. *J. Chem. Soc. Chem. Commun.* **1994**, 809–810. [CrossRef]

8. Epple, M. Gaining insight into structural changes with dynamic diffraction methods. *Thermochim. Acta* **1995**, *269–270*, 33–42. [CrossRef]

9. Fogg, A.M.; O'Hare, D. Study of the intercalation of lithium salt in gibbsite using time-resolved in situ X-ray diffraction. *Chem. Mater.* **1999**, *11*, 1771–1775. [CrossRef]

10. Francis, R.J.; O'Brien, S.; Fogg, A.M.; Halasyamani, P.S.; O'Hare, D.; Loiseau, T.; Férey, G. Time-Resolved In situ Energy and Angular Dispersive X-ray Diffraction Studies of the Formation of the Microporous Gallophosphate ULM-5 under Hydrothermal Conditions. *J. Am. Chem. Soc.* **1999**, *121*, 1002–1015. [CrossRef]

11. Walton, R.I.; Loiseau, T.; O'Hare, D.; Férey, G. An in Situ Energy-Dispersive X-ray Diffraction Study of the Hydrothermal Crystallizations of Open-Framework Gallium Oxyfluorophosphates with the ULM-3 and ULM-4 Structures. *Chem. Mater.* **1999**, *11*, 3201–3209. [CrossRef]

12. Walton, R.I.; Hibble, S.J. A combined in situ X-ray absorption spectroscopy and X-ray diffraction study of the thermal decomposition of ammonium tetrathiotungstate. *J. Mater. Chem.* **1999**, *9*, 1347–1355. [CrossRef]

13. Thomas, J.M. Design, Synthesis, and In Situ Characterization of New Solid Catalysts. *Angew. Chem. Int. Ed.* **1999**, *38*, 3588–3628. [CrossRef]

14. Walton, R.I.; O'Hare, D. Watching solids crystallise using in situ powder diffraction. *Chem. Commun.* **2000**, 2283–2291. [CrossRef]

15. Gualtieri, A.F. Synthesis of sodium zeolites from a natural halloysite. *Phys. Chem. Miner.* **2001**, *28*, 719–728. [CrossRef]

16. Engelke, L.; Schaefer, M.; Schur, M.; Bensch, W. In Situ X-ray Diffraction Studies of the Crystallization of Layered Manganese Thioantimonates(III) under Hydrothermal Conditions. *Chem. Mater.* **2001**, *13*, 1383–1390. [CrossRef]

17. Engelke, L.; Schaefer, M.; Porsch, F.; Bensch, W. In situ Energy-Dispersive X-ray Diffraction Studies of Crystal Growth and Compound Conversion under Solvothermal Conditions. *Eur. J. Inorg. Chem.* **2003**, *2003*, 506–513. [CrossRef]

18. Kiebach, R.; Schaefer, M.; Porsch, F.; Bensch, W. In situ Energy Dispersive X-ray Diffraction Studies of the Crystallization of $(1,2-DAPH_2)_2Ge_9(OH)_4O_{18}\cdot 2H_2O$ under Solvothermal Conditions. *Z. Anorg. Allg. Chem.* **2005**, *631*, 369–374. [CrossRef]

19. Kiebach, R.; Pienack, N.; Ordolff, M.-E.; Studt, F.; Bensch, W. Combined In Situ EDXRD/EXAFS Investigation of the Crystal Growth of $[Co(C_6H_{18}N_4)][Sb_2S_4]$ under Solvothermal Conditions: Two Different Reaction Pathways Leading to the Same Product. *Chem. Mater.* **2006**, *18*, 1196–1205. [CrossRef]

20. Beale, A.M.; Sankar, G. Understanding the Crystallization of Nanosized Cobalt Aluminate Spinel from Ion-Exchanged Zeolites Using Combined in Situ QEXAFS/XRD. *Chem. Mater.* **2006**, *18*, 263–272. [CrossRef]

21. O'Brien, M.G.; Beale, A.M.; Weckhuysen, B.M. The role of synchrotron radiation in examining the self-assembly of crystalline nanoporous framework materials: From zeolites and aluminophosphates to metal organic hybrids. *Chem. Soc. Rev.* **2010**, *39*, 4767–4782. [CrossRef] [PubMed]

22. Newton, M.A.; van Beek, W. Combining synchrotron-based X-ray techniques with vibrational spectroscopies for the in situ study of heterogeneous catalysts: A view from a bridge. *Chem. Soc. Rev.* **2010**, *39*, 4845–4863. [CrossRef] [PubMed]

23. Bentrup, U. Combining in situ characterization methods in one set-up: Looking with more eyes into the intricate chemistry of the synthesis and working of heterogeneous catalysts. *Chem. Soc. Rev.* **2010**, *39*, 4718–4730. [CrossRef] [PubMed]

24. Laumann, A.; Ørnsbjerg Jensen, K.M.; Tyrsted, C.; Bremholm, M.; Fehr, K.T.; Holzapfel, M.; Iversen, B.B. In situ Synchrotron X-ray Diffraction Study of the Formation of Cubic Li_2TiO_3 under Hydrothermal Conditions. *Eur. J. Inorg. Chem.* **2011**, *2011*, 2221–2226. [CrossRef]

25. Millange, F.; El Osta, R.; Medina, M.E.; Walton, R.I. A time-resolved diffraction study of a window of stability in the synthesis of a copper carboxylate metal–organic framework. *CrystEngComm* **2011**, *13*, 103–108. [CrossRef]

26. Tyrsted, C.; Pauw, B.R.; Jensen, K.M.O.; Becker, J.; Christensen, M.; Iversen, B.B. Watching nanoparticles form: An in situ (small-/wide-angle X-ray scattering/total scattering) study of the growth of yttria-stabilised zirconia in supercritical fluids. *Chem. Eur. J.* **2012**, *18*, 5759–5766. [CrossRef] [PubMed]

27. Feyand, M.; Hubner, A.; Rothkirch, A.; Wragg, D.S.; Stock, N. Copper phosphonatoethanesulfonates: Temperature dependent in situ energy dispersive X-ray diffraction study and influence of the pH on the crystal structures. *Inorg. Chem.* **2012**, *51*, 12540–12547. [CrossRef] [PubMed]

28. Feyand, M.; Koppen, M.; Friedrichs, G.; Stock, N. Bismuth tri- and tetraarylcarboxylates: Crystal structures, in situ X-ray diffraction, intermediates and luminescence. *Chem. Eur. J.* **2013**, *19*, 12537–12546. [CrossRef] [PubMed]

29. Niekiel, F.; Ackermann, M.; Guerrier, P.; Rothkirch, A.; Stock, N. Aluminum-1,4-cyclohexanedicarboxylates: High-throughput and temperature-dependent in situ EDXRD studies. *Inorg. Chem.* **2013**, *52*, 8699–8705. [CrossRef] [PubMed]

30. El Osta, R.; Feyand, M.; Stock, N.; Millange, F.; Walton, R.I. Crystallisation Kinetics of Metal Organic Frameworks From in situ Time-Resolved X-ray Diffraction. *Powder Diffr.* **2013**, *28*, S256–S275. [CrossRef]

31. Schilling, L.-H.; Stock, N. High-throughput ultrasonic synthesis and in situ crystallisation investigation of metal phosphonocarboxylates. *Dalton Trans.* **2014**, *43*, 414–422. [CrossRef] [PubMed]

32. Pienack, N.; Terraschke, H.; Bensch, W. In situ Crystallization Cell: Developments and First Results of the Model System $Al(acac)_3$. *Z. Anorg. Allg. Chem.* **2016**, *1040*. [CrossRef]

33. Hon, P.K.; Pfluger, C.E. The Crystal and Molecular Structure of Tris(Acetylacetonato)-aluminum(III) and -Cobalt (III). *J. Coord. Chem.* **1973**, *3*, 67–76. [CrossRef]

34. McClelland, B.W. γ-Tris(2,4-pentanedionato)aluminum(III). *Acta Crystallogr. B Struct. Crystallogr. Cryst. Chem.* **1975**, *31*, 2496–2498. [CrossRef]

35. Von Chrzanowski, L.S.; Lutz, M.; Spek, A.L. alpha-Tris(2,4-pentanedionato-kappa(2)O,O')aluminum(III) at 240, 210, 180, 150 and 110 K: A new delta phase at 110 K. *Acta Crystallogr. C* **2007**, *63*, m129–m134. [CrossRef] [PubMed]

36. Shirodker, M.; Borker, V.; Näther, C.; Bensch, W.; Rane, K.S. Synthesis and structure of tris(acetylacetonato) aluminum(III). *Indian J. Chem.* **2010**, *49*, 1607–1611.

37. Amini, S.K.; Tafazzoli, M. DFT calculations as a powerful technique to probe the crystal structure of Al(acac)$_3$. *Magn. Reson. Chem.* **2008**, *46*, 1045–1050. [CrossRef] [PubMed]

38. Niu, S.-Y.; Chen, D.-N.; Jin, J.; Yu, Z.-J. Crystal Structure and Luminescent Performance Al-acac Complex. *Liaoning Shifan Daxue Xuebao Ziran Kexueban* **2005**, *1*, 69–72.

39. Okumura, T.; Ikagawa, T.; Otsuka, T.; Kaizu, Y. Cell-expansion of Tris(2,4-pentanedionato)chromium and -aluminum under Light Irradiation. *Chem. Lett.* **1998**, 231–232. [CrossRef]

40. Riesen, H.; Dubicki, L. Probing the R lines in tris(acetylacetonato) chromium(III) and tris(3-bromo-acetylacetonato) chromium(III) by luminescence and excitation line narrowing spectroscopy. *J. Phys. Chem. A* **2008**, *112*, 10287–10293. [CrossRef] [PubMed]

41. Semyannikov, P.P.; Igumenov, I.K.; Trubin, S.V.; Chusova, T.P.; Semenova, Z.I. Thermodynamics of sublimation of aluminium triacetylacetonate. *Thermochim. Acta* **2006**, *451*, 80–83. [CrossRef]

42. Hafshejani, L.D.; Tangsir, S.; Koponen, H.; Riikonen, J.; Karhunen, T.; Tapper, U.; Lehto, V.-P.; Moazed, H.; Naseri, A.A.; Hooshmand, A. Synthesis and characterization of Al$_2$O$_3$ nanoparticles by flame spray pyrolysis (FSP)—Role of Fe ions in the precursor. *Powder Technol.* **2016**, *298*, 42–49. [CrossRef]

43. Ortiz, A.; Alonso, J.C.; Pankov, V.; Huanosta, A.; Andrade, E. Characterization of amorphous aluminum oxide films prepared by the pyrosol process. *Thin Solid Films* **2000**, *368*, 74–79. [CrossRef]

44. Ita, B.I. Synthesis and X-ray diffraction studies of Al$_2$O$_3$ using aluminium acetylacetonate precursor via a sol-gel route. *Glob. J. Pure Appl. Sci.* **2001**, *7*, 81–84. [CrossRef]

45. Kim, J.S.; Marzouk, H.A.; Reucroft, P.J.; Robertson, J.D.; Hamrin, C.E. Fabrication of aluminum oxide thin films by a low-pressure metalorganic chemical vapor deposition technique. *Appl. Phys. Lett.* **1993**, *62*, 681. [CrossRef]

46. Gong, H.; Wang, Y.; Luo, Y. Nanocrystalline p-type transparent Cu–Al–O semiconductor prepared by chemical-vapor deposition with Cu(acac)$_2$ and Al(acac)$_3$ precursors. *Appl. Phys. Lett.* **2000**, *76*, 3959. [CrossRef]

47. Yu, Y.; Zhang, Y.; Yang, J.; Tang, M. Synthesis and Characterization of Ceramic Precursor Aluminum-Containing Polycarbosilane and its Pyrolysis. *J. Inorg. Organomet. Polym.* **2007**, *17*, 569–575. [CrossRef]

48. Yu, Y.; Li, X.; Cao, F. Synthesis and characterization of polyaluminocarbosilane. *J. Mater. Sci.* **2005**, *40*, 2093–2095. [CrossRef]

49. Lane, G.A. Metal salts of beta-diketones as charging additives: A mechanistic study. In Proceedings of the SPIE 1253, Hard Copy and Printing Materials, Media, and Processes, Santa Clara, CA, USA, 1 July 1990; pp. 29–36.

50. Wang, J.T.-W.; Wang, Z.; Pathak, S.K.; Zhang, W.; de Quilettes, D.; Wisnivesky, F.; Huang, J.; Nayak, P.; Patel, J.; Yusof, H.; et al. Efficient Perovskite Solar Cells by Metal Ion Doping. *Energy Environ. Sci.* **2016**. [CrossRef]

51. Santa-Cruz, P.A.; Teles, F.S. *SpectraLux Software v. 2.0: Ponto Quântico Nano-Dispositivos*; RENAMI: Recife, Brazil, 2003.

52. Hesse, M.; Meier, H.; Zeeh, B. *Spektroskopische Methoden in der Organischen Chemie*, 7., überarb. Aufl. ed; Thieme: Stuttgart, Germany, 2011. (In German)

53. Hesse, M.; Bienz, S.; Meier, H.; Zeeh, B. *Spektroskopische Methoden in der Organischen Chemie. 114 Tabellen*, 8., überarb. und erw. Aufl. ed; Thieme: Stuttgart, Germany, 2012. (In German)

54. Max, J.-J.; Chapados, C. Aqueous ammonia and ammonium chloride hydrates: Principal infrared spectra. *J. Mol. Struct.* **2013**, *1046*, 124–135. [CrossRef]

55. Hof, M.; Hutterer, R.; Fidler, V. *Fluorescence Spectroscopy in Biology. Advanced Methods and Their Applications to Membranes, Proteins, DNA, and Cells*; Springer: Berlin, Germany, 2005.

56. Heidenreich, N. Unpublished Results. 2016.

57.　Schell, N.; King, A.; Beckmann, F.; Fischer, T.; Müller, M.; Schreyer, A. The High Energy Materials Science Beamline (HEMS) at PETRA III. *Mater. Sci. Forum* **2013**, *772*, 57–61. [CrossRef]

58.　Strempfer, J.; Francoual, S.; Reuther, D.; Shukla, D.K.; Skaugen, A.; Schulte-Schrepping, H.; Kracht, T.; Franz, H. Resonant scattering and diffraction beamline P09 at PETRA III. *J. Synchrotron Radiat.* **2013**, *20*, 541–549. [CrossRef] [PubMed]